Dynamic correlation functions and Boltzmann-Langevin approach for driven one-dimensional lattice gas

Paolo Pierobon,[1,2] Andrea Parmeggiani,[3] Felix von Oppen,[4] and Erwin Frey[1,2]

[1]*Arnold Sommerfeld Center and CeNS, Department of Physics, Ludwig-Maximilians-Universität München, Theresienstrasse 37, D-80333 München, Germany*

[2]*Hahn-Meitner Institut, Abteilung Theorie, Glienicker Street 100, D-14109 Berlin, Germany*

[3]*Dynamique Moléculaire des Interactions Membranaires, CNRS-UMR5539, CC107, Place Eugéne Bataillon, 34095 Montpellier Cedex 05, France*

[4]*Fachbereich Physik, Freie Universität Berlin, Arnimallee 14, D-14195 Berlin, Germany*

We study the dynamics of the totally asymmetric exclusion process with open boundaries by phenomenological theories complemented by extensive Monte Carlo simulations. Upon combining domain wall theory with a kinetic approach known as Boltzmann-Langevin theory we are able to give a complete qualitative picture of the dynamics in the low- and high-density regimes and at the corresponding phase boundary. At the coexistence line between high- and low-density phases we observe a time scale separation between local density fluctuations and collective domain wall motion, which are well accounted for by the Boltzmann-Langevin and domain wall theory, respectively. We present Monte Carlo data for the correlation functions and power spectra in the full parameter range of the model.

PACS number(s): 02.50.Ey, 05.60.−k, 05.40.−a, 87.10+e

I. INTRODUCTION

One-dimensional driven lattice gases are an interesting field of nonequilibrium statistical mechanics where collective effects give rise to unexpected nontrivial behavior such as phase transitions, pattern formation, long-range order, and anomalous diffusion. In this class of problems the totally asymmetric simple exclusion process (TASEP) represents an exactly solvable case which proved to model some generic features of several systems from a rather diverse range of fields: biological transport phenomena (e.g., ribosomes moving on mRNA tracks [1] and molecular motors moving along microtubules [2,3]), traffic [4], single-file diffusion [5], and even economics [6].

In the TASEP one considers a system of identical particles moving unidirectionally with a constant rate along a finite one-dimensional lattice with sites labeled by $i=1,\dots,N$ (see Fig. 1). The lattice spacing is $a=L/N$ with L being the total length of the system. The microscopic state of the system is characterized by occupation numbers n_i which are binary variables with only two possible values $n_i \in \{0,1\}$; i.e., we impose a hard-core repulsion between the particles. Of particular interest are systems with open boundaries, where particles enter the system at the left end with a rate α and leave at the right end with a rate β. Moreover, we use sequential dynamics, appropriate for biological systems, where each particle moves according to an "internal clock;" a parallel update would be more realistic for vehicular traffic.

The stationary state (current and density profiles) of this driven lattice gas model has been studied in great detail over the last years (for recent reviews, see, e.g., Refs. [7,8]). In open systems it has been found by some exact methods [9–11] that there are three different phases: a high-density, a low-density, and a maximal-current phase; compare Fig. 1. The coexistence line $\alpha = \beta < 1/2$ marks a discontinuous tran-

sition between the high- and low-density phases, while along the lines $\alpha = 1/2 \leqslant \beta$ and $\beta = 1/2 \leqslant \alpha$ the transitions are continuous. There are interesting correlation effects reflected in the shape of the density profiles at the boundaries. It is only along the disorder line, $\alpha + \beta = 1$, where the density profile is flat.

The dynamic properties of the TASEP model are much less studied. For closed systems exact analytical results [12–15] have been derived for the largest relaxation time τ. It is found that τ diverges with system size as $\tau \propto L^z$ with a dynamic exponent of $z = 3/2$. For open systems no exact results are available. The spectrum of relaxation times has been studied for small systems using exact enumeration techniques [16,17]. More recently, density matrix renormalization group studies [18] have shown that the largest relaxation times are finite unless $\alpha = \beta = 1/2$, where $\tau \propto L^{3/2}$ as for the periodic system; the results also indicate that $z = 3/2$ in the whole maximal-current phase. These studies also confirm the results of a phenomenological approach known as domain
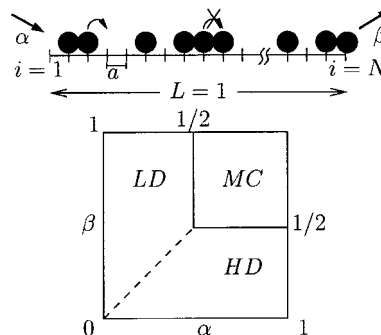

FIG. 1. (a) Cartoon of the TASEP model and (b) phase diagram as a function of the entrance and exit rates α and β, respectively, showing the low-density (LD), high-density (HD), and maximal-current (MC) phases.

wall theory [17,19]. In this coarse-grained description of the dynamics it is assumed that each particle reservoir at the system's boundary independently fixes a density. The two domains are then joined in the bulk by a phase boundary (domain wall), which performs a random walk due to the randomness of particle flux at the boundaries; the domain wall (DW) moves left whenever a particle enters the system and right whenever a particle exits the system. Along the coexistence line the DW theory accounts even for the power spectrum at small frequencies (long time) [20].

DW theory does not describe the dynamics of local density fluctuations. This is evident for periodic systems where the average density profile is flat. In this case it has been shown that the dynamics of the TASEP model maps onto the noisy Burgers equation [21]. It is actually this mapping which allows for the implementation of some exact methods such as the Bethe ansatz [13]. Further progress has also been made upon using mode coupling [22] and renormalization group [23] theories.

This correspondence between the lattice gas model and a Langevin equation for the periodic case suggests to look for a similar mapping for open systems. In this context, it is useful to recall a successful method in quantum many-body systems, known as Boltzmann-Langevin (BL) equations. This approach, which was first introduced to describe electron transport in the presence of disorder and phonon scattering [24,25], describes not only the average of the electronic distribution function, but also its fluctuations. This is achieved by amending the Boltzmann kinetic equation with a Langevin source which takes the stochastic nature of collisions into account. In the context of electronic transport through nanostructures, this method has recently been widely employed in studies of shot noise (for a review see [26]). A close analogy with the lattice-gas model studied in this paper arises for the following reason: the requirement of no double occupation of sites has its direct analog in the Pauli principle which forbids double occupation of electronic states.

The outline of the paper is the following. In the following section we will discuss how the Boltzmann-Langevin approach can be applied for the TASEP model and calculate the correlation function of the linearized version. Interestingly, it will turn out that the resulting Boltzmann-Langevin equation reduces to the noisy Burgers equation for $\alpha=\beta=1/2$. In Sec. III we give a short description of the Monte Carlo methods used to analyze the correlation functions of the TASEP model. Results obtained from these simulations are compared with the analytical results from the Boltzmann-Langevin and the DW theories in Sec. IV. Finally, we present a short summary and some outlook. In Appendix A we give a thorough discussion of the behavior of the correlation function right at the critical point.

II. STOCHASTIC EQUATIONS OF MOTION

At a given time t the microscopic state of the system is characterized in terms of occupation numbers $\{n_i=0,1\}$. The dynamics, which we described as a set of rules in the previous section, can be formulated in terms of a *quantum Hamiltonian representation* [27–29]. In the bulk the corresponding

Heisenberg equations for the occupation number operators $n_i(t)$ have the form of a lattice continuity equation

$$\partial_t n_i(t) = J_{i-1}(t) - J_i(t), \tag{1a}$$

with the current operator

$$J_i(t) = n_i(t)[1 - n_{i+1}(t)]. \tag{1b}$$

The effect of the entrance and exit rates is equivalent to constant particle reservoirs of density α and $1-\beta$ at auxiliary sites $i=0$ and $i=N+1$, respectively.

There are several levels of approximation in dealing with the dynamics of the system. If correlation effects are neglected altogether, one arrives at a set of rate equations for the average particle density, $\rho_i(t)=\langle n_i(t)\rangle$, which have a form identical to Eq. (1) with n_i replaced by ρ_i. To arrive at these equations one has to take the average of Eq. (1) and neglect correlations in the spirit of a mean-field or a random phase approximation

$$\langle n_i(t) n_{i+1}(t)\rangle \rightarrow \langle n_i(t)\rangle\langle n_{i+1}(t)\rangle. \tag{2}$$

Then, in the stationary limit the rate equations are equivalent to a nonlinear map

$$\bar\rho_i(1 - \bar\rho_{i+1}) = J, \tag{3}$$

with a constant stationary current J. Upon exploiting the properties of this map one can easily reproduce the full phase diagram of the TASEP [1]. Actually, it turns out that the phase diagram [9] obtained in this way is identical to the one obtained from an exact solution of the TASEP in the stationary limit [10,11]. The density profiles obtained from such a mean-field approach miss correlation effects, especially in the maximal-current phase, and the fluctuations of the domain walls.

A. Boltzmann-Langevin approach

To go beyond rate equations we follow a line of arguments which leads to what is known as BL equations in studies of nonequilibrium transport in electron systems [24,25]. The right-hand side of Eq. (1a) has a form similar to the *collision integral for impurity scattering* in the Boltzmann equation, balancing ingoing and outgoing currents. In order to account for fluctuation effects around the stationary state, we express both the current and density as the sum of a deterministic and a fluctuating part:

$$n_i \approx \bar\rho_i + \delta\rho_i \equiv \rho_i, \tag{4a}$$

$$J_i \approx \rho_i(1 - \rho_{i+1}) + \delta J_i. \tag{4b}$$

Since we will use the BL approach only for those regions in the phase diagram where the stationary density is to a good approximation spatially constant, we may set $\bar\rho_i=\bar\rho$. This applies for both the high- and low-density phases, but not for the phase boundary $\alpha=\beta\leq\frac{1}{2}$, where in addition to density fluctuations on small scales we also have domain wall motion on large scales. The latter modes are obviously not accounted for in the BL formulation. One also has to be cautious in the maximal-current phase where boundary layer

profiles decay only algebraically as one moves from the boundaries towards the bulk [9].

Upon inserting Eq. (4) into the equations of motion (1), we find a coupled set of Langevin equations for the density fluctuations at each site of the lattice:

$$\partial_t \delta\rho_i(t) = (1 - \bar{\rho})[\delta\rho_{i-1} - \delta\rho_i] - \bar{\rho}[\delta\rho_i - \delta\rho_{i+1}]$$
$$+ \delta\rho_i(\delta\rho_{i+1} - \delta\rho_{i-1}) - (\delta J_i - \delta J_{i-1}). \quad (5)$$

In order to close these equations we still need to specify the current fluctuations δJ_i. This can be done by exploiting the fact that the occupation numbers are binary variables, which immediately implies that $J_i^2 = J_i$.[1] Hence the variance of the current at a particular site is given by $\text{Var}[J_i] = \langle J_i\rangle(1 - \langle J_i\rangle)$. To be consistent with the approximations already made, we set $\langle J_i\rangle \approx \bar{\rho}(1 - \bar{\rho})$ and finally get

$$\text{Var}[J] = \bar{\rho}(1 - \bar{\rho})[1 - \bar{\rho}(1 - \bar{\rho})]. \quad (6)$$

Our final assumption is that correlations in the current fluctuations are short ranged in space and time such that we can write

$$\langle \delta J_i(t)\delta J_j(t')\rangle = \text{Var}[J]\delta_{ij}\delta(t - t'). \quad (7)$$

Note that local current fluctuations are due to the fact that each particle advances randomly at a given rate (set equal to 1), with an exponential distribution of waiting times (in the low density limit).

B. Gradient expansion

We will now derive a continuous version of the discrete BL equations, Eq. (5). To this end we set $x = ia$ and introduce fields $\phi(x,t) = \delta\rho_i(t)$ and $\eta(x,t) = \delta J_i(t)$ for the density and current fluctuations, respectively. Then we get, to leading order in a gradient expansion,

$$\partial_t \phi(x,t) + (v - 2\phi)\partial_x \phi = \tfrac{1}{2}\partial_x^2 \phi - \partial_x \eta, \quad (8)$$

where from now on we measure all length scales in units of the lattice spacing a. Equation (8) has previously been derived along similar lines in Ref. [30]. The noise correlations are given by

$$\langle \eta(x,t)\eta(x',t')\rangle = A\delta(x - x')\delta(t - t'), \quad (9)$$

with an amplitude $A = \bar{\rho}(1 - \bar{\rho})[1 - \bar{\rho}(1 - \bar{\rho})]$. We have also introduced the collective velocity $v = 1 - 2\bar{\rho}$, which happens to coincide with the expression obtained from the exact non-equilibrium fluctuation-dissipation theorem $v = \partial_\rho J(\rho)$ of an infinite lattice gas [19]. Note that v changes sign at $\bar{\rho} = \tfrac{1}{2}$ where the stationary current becomes maximal.

The convective nonlinearity $\phi\partial_x \phi$ in Eq. (8) can be read as a "shift" in the collective velocity due to fluctuations, which we expect to become important for small v—i.e., close to the phase boundaries between the low- and high-density phases and the maximal-current phase. For densities

---

[1]Note that our derivation *differs* from the argument used in the conventional Boltzmann-Langevin theory. The latter would only yield the low-current approximation $\text{Var}[J_i] = \langle J_i\rangle$.

far away from $\bar{\rho} = 1/2$ we will neglect those nonlinearities. Then, as will be discussed in the next subsection, one can work out all the correlation functions explicitly. These will then be used as a guidance for the discussion of the Monte Carlo results in Sec. IV.

For $\bar{\rho} = \tfrac{1}{2}$, Eq. (8) is identical to the one-dimensional *Burgers equation* [23], which can be mapped onto the Kardar-Parisi-Zhang (KPZ) [31] equation upon introducing a new field h via $\phi = \partial_x h$. The Burgers equation is known to give the following scaling form for the correlation function $C(x,t) = \langle \phi(x,t)\phi(0,0)\rangle$ [23]:

$$C(x,t) = x^{2\chi-2}F(t/x^z). \quad (10)$$

Here the roughness exponent χ describes the scaling of the width of the interface and the dynamic exponent z characterizes the spread in time of disturbances on the surface. In the present case the roughness and the dynamic exponent are known to be [23]

$$\chi = \tfrac{1}{2}, \quad \text{and } z = \tfrac{3}{2}. \quad (11)$$

This basically means that the system at the critical point relaxes superdiffusively—i.e., $C(0,t) \sim t^{-1/z}$ with $z < 2$.

C. Correlation functions of the linearized Boltzmann-Langevin equation

The linearized Boltzmann-Langevin equation is most conveniently analyzed in Fourier space, where it reads

$$\left[i\omega - ivq + \tfrac{1}{2}q^2\right]\phi(q,\omega) = iq\,\eta(q,\omega). \quad (12)$$

From this one can immediately infer, for the correlation function $C(x - x', t - t') = \langle \phi(x,t)\phi(x',t')\rangle$ in Fourier space,

$$C(q,\omega) = \frac{Aq^2}{(\omega - vq)^2 + \dfrac{1}{4}q^4} \quad (13)$$

and, for direct space,

$$C(x,t) = \frac{A}{\sqrt{2\pi|t|}}\exp\left[-\frac{(x - vt)^2}{2|t|}\right]. \quad (14)$$

Note that $C(x,t)$ is a Gaussian whose center moves with a drift velocity $v = 1 - 2\bar{\rho}$ and which broadens diffusively starting from a δ function at $t = 0$; height $H(t)$ and width $W(t)$ are given by

$$H(t) = \frac{A}{\sqrt{2\pi|t|}}, \quad (15)$$

$$W(t) = 2\sqrt{|t|}. \quad (16)$$

The on-site correlation function decays exponentially for $v \neq 0$,

$$C(0,t) = \frac{A}{\sqrt{2\pi|t|}}\exp\left[-\frac{v^2}{2}|t|\right]. \quad (17)$$

For $v = 0$, $C(0,t)$ scales as $t^{-1/2}$ as well as $C(0,\omega)$ like $\omega^{-1/2}$. Note also that the static limit of the correlation function for the linearized theory is

$$\lim_{\omega \to 0} C(q,\omega) = \frac{4A}{4v^2 + q^2}, \qquad (18)$$

which is identical to the correlation function for a Landau theory in a Gaussian approximation usually found in equilibrium thermodynamics [32]. This result suggests that linearized BL theory can be viewed as the analog of the Gaussian approximation for driven lattice gases. The form of Eq. (18) implies a correlation length of $1/2v$ which diverges at the critical point $\bar{\rho} = 1/2$.

III. MONTE CARLO SIMULATION METHODS

Of course, linearized Boltzmann-Langevin theory is valid only for very low densities (i.e., low values of α). To go beyond this low-density limit and test the range of validity of the linearized BL approach we have performed extensive Monte Carlo (MC) simulations. To this end we have chosen the random sequential updating algorithm by Bortz, Kalos, and, Lebowitz (BKL or n-fold method) [33,34]. Since it keeps a list of all sites which are possible candidates for a successful update, it is (for the present case) faster than conventional methods. Moreover, it constitutes a reliable way to simulate *real-time* dynamics and achieve an excellent quality in terms of data and computational efficiency in both short- and long-time regimes.

In a first step one generates a random number $X \in [0,1)$, which determines which one of the following moves is chosen: a particle entering the system, a particle leaving the system, and particle at site i jumping to the right. Then, for a given move a time interval Δt is chosen from an exponential waiting time distribution, where the decay time depends on the size of the list.

In all of our Monte Carlo runs we started from a configuration generated according to the steady-state distribution in order to reduce initial transient effects. After equilibration correlation functions were measured and moving time averages over $O(10^7)$ time windows were performed. Average profiles and correlations do not show any differences between the moving time and ensemble average, giving explicit proof for the ergodicity of the system.

IV. DYNAMIC CORRELATION FUNCTIONS

In this section we analyze the correlation function $C(x,t)$ of the density fluctuations $\phi(x,t)$ in space and time. From now on we take $x=0$ as the central site of the system such that the system is confined to the interval $[-L/2, L/2]$. This is meant to minimize, at least for short times, the influence of the system boundaries. We assume that the system is in a stationary state at the reference time $t=0$.

As expected from the linearized BL equation, the simulations show that the correlation function starts from a δ function peaked at the reference site and then moves to the right with velocity v and spreads diffusively as time progresses; for negative times it moves to the left (see Fig. 2). Note that our simulations confirm that the peak of the correlation function moves with exactly the collective velocity $v = 1 - 2\bar{\rho}$.
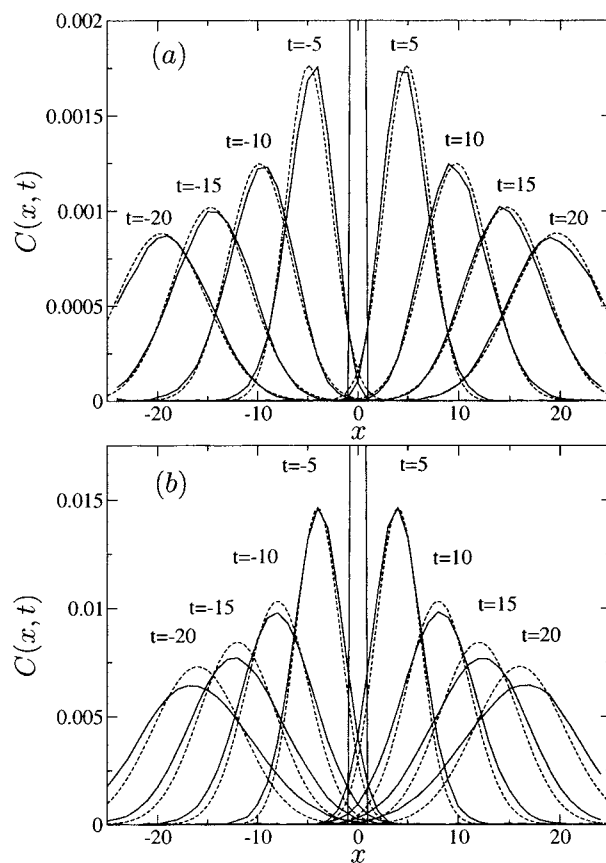

FIG. 2. Time- and space-dependent correlation function for a system of 50 sites with rates (a) $\alpha=0.01$ and $\beta=0.99$ and (b) $\alpha=0.1$ and $\beta=0.9$. Averages are taken over 10^7 samples. For the diluted system there is good agreement between the linearized Boltzmann-Langevin theory (dashed line) and the Monte Carlo simulations (solid line). For denser systems the agreement is only qualitative.

In the following we are going to discuss the form and time evolution of the correlation function in the α-β plane. Our simulations have been performed mainly along the antidiagonal $\alpha = 1 - \beta$. This has the advantage that the exact steady-state profile is perfectly flat, such that boundary effects are greatly reduced; moreover, mean-field theory predicts exactly $\bar{\rho} = \alpha$.

Before we enter the discussion let us have a closer look at the characteristic time scales of the system. Correlation functions decay on a scale [see Eq. (17)]

$$\tau_{\text{relax}} = 2/v^2, \qquad (19)$$

but at the same time the maximum of the correlation function moves with a velocity v such that it propagates the finite length L of the track in a time

$$\tau_{\text{prop}} = \frac{L/2}{v}. \qquad (20)$$

This implies that one can observe the relaxation of the correlation functions only if $\tau_{\text{prop}} / \tau_{\text{relax}} = vL/4 \geqslant 1$—i.e., for rates α and β not too close to the phase boundary to the
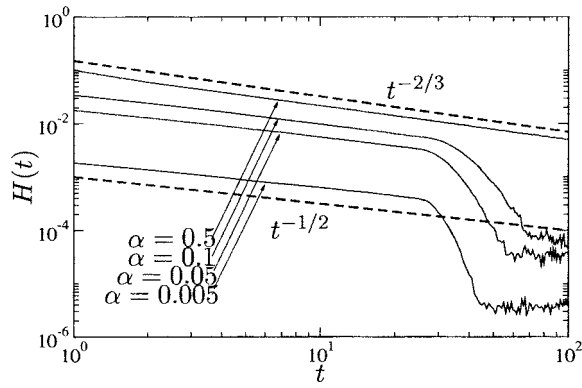
FIG. 3. Peak height of the correlation function for a system of $N=50$ sites and a series of entrance rates $\alpha=0.005, 0.05, 0.1, 0.5$; we have taken $\beta=1-\alpha$. Averages of the MC data are taken over 10^7 samples. Upon approaching the critical point $(\alpha, \beta)=(1/2, 1/2)$ the peak height shows a power-law behavior with an effective exponent slowly changing from $1/2$ to $2/3$, shown as dashed lines in the graph.

maximal-current phase and of course for large enough systems.

A. Low-density and high-density phases

Due to particle-hole symmetry, we restrict our discussion to the low-density regime. The results for the high-density phase are obtained upon simply replacing α by $1-\beta$.

Figure 2 shows time series of the correlation function for entrance rates $\alpha=0.01$ and $\alpha=0.1$. In both cases the correlation functions start from a δ-function peak at $t=0$ which then broadens diffusively with the width scaling as $t^{1/2}$ and the height decreasing as $t^{-1/2}$. Correspondingly the maximum propagates to the right or left with velocity $v=1-2\bar{\rho}$ for $\bar{\rho}<1/2$ and $\bar{\rho}>1/2$, respectively (by particle-hole symmetry). As noted above this is an exact result valid for all values of the entrance and exit rates. In Fig. 2 we have also shown results for negative time to highlight the symmetry $x \to -x$ and $t \to -t$ which appears in Eq. (14).

For low values of α, which corresponds to the low-density limit, the results from the linearized BL equations explain the Monte Carlo results quantitatively. The theory still gives the correct qualitative picture for larger values of α but shows significant quantitative deviations. The actual shapes of the correlation functions have a lower height and are broader than the linearized theory predicts. Nevertheless, the peak height measured in the simulations still shows the $t^{-1/2}$ scaling of the linear theory for values of α not too close to $\alpha=\frac{1}{2}$; see Fig. 3.

As can be inferred from Fig. 3 the effective exponent describing the peak relaxation slowly crosses over from $1/2$ to $2/3$ upon approaching the critical point $(\alpha, \beta)=(1/2, 1/2)$ along the antidiagonal of the phase diagram. The exponent $2/3$ is identical to the inverse of the dynamic exponent $1/z$ of the nonlinear BL equation (Burgers equation); see Eqs. (8) and (11).

B. Coexistence line ($\alpha=\beta<1/2$)

At the coexistence line the density profile is characterized by a fluctuating domain wall separating a low-density from a
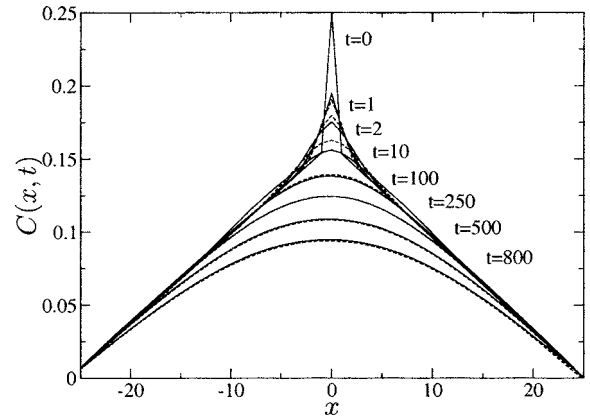

FIG. 4. Time series of the correlation function $C(x,t)$ versus x for $\alpha=0.1$ and $\beta=0.1$; the times are indicated in the graph. The MC data for a system with $N=50$ sites (solid lines) are compared with a hybrid theory combining local density fluctuations described by the Boltzmann-Langevin equation and the collective domain wall motion (dashed lines). Averages in the MC data are taken over 10^7 samples.

high-density phase. The dynamics of the domain wall can be described as a symmetric random walk with reflecting boundary conditions [8,19]. In addition to the domain wall motion, a collective mode, there are still stochastic fluctuations of the density in the low- and high-density wings of the domain wall. Both of these modes should be visible in a measurement of the density-density correlation function.

Indeed, the profile of the correlation function shows two distinct features; see Fig. 4. At $t=0$ there is a sharp triangle on top of a much broader triangular base. The sharp tip is a result of the local density (BL) fluctuations and can be explained as follows. Consider the correlation function of local density fluctuations $C_{ij}^{BL}(t)=\langle \phi_i(t) \phi_j(0) \rangle$ on a lattice. Since there are no correlations in the bulk of the system for $t=0$, it reduces to $C_{ij}^{BL}(0)=(\langle n_i^2 \rangle - \langle n_i \rangle^2)\delta_{ij}$. Finally, upon using the fact that the occupation numbers are binary variables and the average density in the middle of the system is $\langle n_0 \rangle = \frac{1}{2}$, we obtain $C_{i0}^{BL}=\frac{1}{4}\delta_{i0}$. The width of the sharp tip is actually a finite-size effect resulting from the linear interpolation of the data points. The broader triangular base is explained below in the context of DW theory.

The MC simulations show that the sharp tip quickly relaxes and broadens, whereas the shape of the triangular base evolves on a much larger time scale.

One can rationalize this behavior upon combining results from the DW and BL theories. We start with a discussion of the local density fluctuations. One can derive the short-time dynamics for the correlation function from the lattice version of the BL equation, Eq. (5), imposing the initial condition $C_{i0}^{BL}(t=0)=\frac{1}{4}\delta_{i0}$. As explicitly shown in Appendix B one finds for the on-site correlation function $C_{00}^{BL}(t) \sim \frac{1}{4} - \frac{1}{4}|t| + O(t^2)$, while the nearest- and next-nearest-neighbor correlation functions read as $C_{01}^{BL}(t) \sim t$ and $C_{02}^{BL}(t) \sim t^2$. This explains the fast relaxation of the central peak.

In order to understand the broadening of the triangular base we first have to recapitulate some key results of the DW theory [17,19]. Since one can model the domain wall as a

symmetric random walker with reflecting boundary conditions at both ends of the system, the conditional probability of finding the domain wall at site ξ_t at time t given that it was at site ξ_0 at time $t=0$ reads [35]

$$P(\xi_t|\xi_0) = \frac{1}{L} + \frac{2}{L}\sum_{i:\text{even}} e^{-\lambda_i^2 \mathcal{D}t} \cos\lambda_i\xi_t \cos\lambda_i\xi_0$$

$$+ \frac{2}{L}\sum_{i:\text{odd}} e^{-\lambda_i^2 \mathcal{D}t} \sin\lambda_i\xi_t \sin\lambda_i\xi_0, \qquad (21)$$

where $\lambda_i = i\pi/L$ and $\mathcal{D} = \alpha(1-\alpha)/(1-2\alpha)$ is the diffusion constant. Note that this diffusion coefficient is smaller than the one of the BL fluctuations (which is 1), $\mathcal{D} \sim \alpha < 1$, which explains the time-scale separation mentioned above. Averages of an observable $\mathcal{O}$ are understood as integrals over the random variable ξ_t:

$$\langle\mathcal{O}(t,t')\rangle = \int d\xi_t \int d\xi_{t'} P_{\text{st}}(\xi_{t'})\mathcal{O}(t,t')P(\xi_t|\xi_{t'}), \quad (22)$$

where $P_{\text{st}}(\xi)$ is the stationary probability distribution function. In the present case it is simply a constant, $P_{\text{st}} = 1/L$.

If one approximates the density profile of the domain wall by a step function $\psi(x,t) = \alpha + (1-2\alpha)\theta(x-\xi_t)$, the correlation function can easily be calculated as

$$C^{\text{DW}}(x,x',t-t') = \langle\psi_d(x,t)\psi_d(x',t')\rangle - \langle\psi_d(x,t)\rangle\langle\psi_d(x',t')\rangle$$

$$= \frac{2(1-2\alpha)^2}{L^2}\Bigg[\sum_{i:\text{even}} \frac{e^{-\lambda_i^2\mathcal{D}|t-t'|}}{\lambda_i^2}\cos\lambda_i x$$

$$\times\cos\lambda_i x' + \sum_{i:\text{odd}} \frac{e^{-\lambda_i^2\mathcal{D}|t-t'|}}{\lambda_i^2}\sin\lambda_i x$$

$$\times\sin\lambda_i x'\Bigg]. \qquad (23)$$

Here we are mainly interested in the dynamics at time scales $t < L^2/\mathcal{D}$ (so that the system size is large, $L^2 > t\mathcal{D}$, and λ_i is infinitesimal), where the domain wall has not explored the full system yet. Then the sum in Eq. (23) can be approximated by an integral, and one finds

$$C^{\text{DW}}(x,t) = \frac{1}{2L}(1-2\alpha)^2\Bigg\{\Bigg[|x+L|\text{Erf}\Bigg(\frac{|x+L|}{\sqrt{4\mathcal{D}|t|}}\Bigg)$$

$$- |x|\text{Erf}\Bigg(\frac{|x|}{\sqrt{4\mathcal{D}|t|}}\Bigg)\Bigg] + (e^{-(x+L)^2/4\mathcal{D}|t|}$$

$$- e^{-x^2/4\mathcal{D}|t|})\sqrt{\frac{4\mathcal{D}|t|}{\pi}} - \Bigg(x+\frac{L}{2}\Bigg)\Bigg\}. \qquad (24)$$

In the limit $t \to 0$ this exactly reduces to the profile of the broad triangular base in Fig. 4. If one would be allowed to just sum the correlation functions obtained from domain wall and local density fluctuations, this would fully explain the initial shape of the correlation function. Of course, this is not valid rigorously but seems to be a reasonable approximation. One may argue that the validity of the approximation is due to the time- and length-scale separation between the local
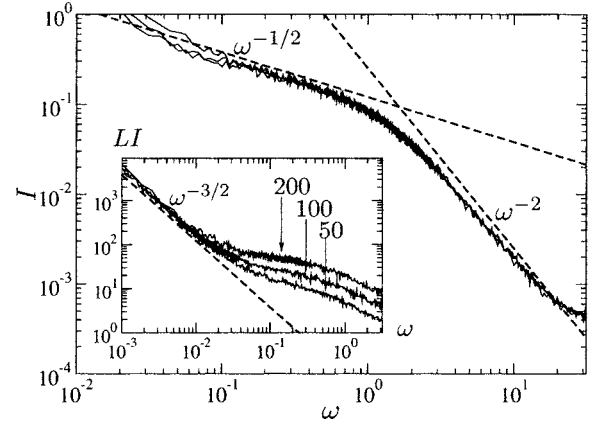

FIG. 5. Power spectrum for systems of 200, 100, and 50 sites and rates $\alpha=\beta=0.1$. Averages are taken over 256 samples. The large-frequency behavior is dominated by local density fluctuations and well described within a BL theory, while the small-frequency regime is dominated by domain wall fluctuations, as a collective mode. The high resolution allows for the identification of a dynamic regime due to the discrete nature of density fluctuations at very short time. Inset: rescaled power spectrum showing the long-time (small-frequency) regime dominated by the DW dynamics.

density fluctuations and the collective domain wall motion.

In this spirit we assume that the total density fluctuations Φ can be written as a superposition of local density and domain wall fluctuations, $\Phi(x,t) = \phi(x,t) + \psi(x,t)$, and that these fluctuations are uncorrelated, $\langle\phi\psi\rangle = \langle\phi\rangle\langle\psi\rangle$. Then the full correlation function can be written as a sum

$$C(x,t) = C^{\text{BL}}(x,t) + C^{\text{DW}}(x,t), \qquad (25)$$

with $C^{\text{DW}}(x,t)$ given by Eq. (24), and the local density correlations $C^{\text{BL}}(x,t)$ are obtained either from the continuous or lattice BL equations depending on the time scale. Note that the density fluctuations on both wings of the domain wall are the same since the average low ($\rho_- = \alpha$) and high ($\rho_+ = 1-\alpha$) densities lead to the same noise amplitude A. Hence we may describe these local density fluctuations by a BL equation with $v=0$ and $A = \alpha(1-\alpha)[1-\alpha(1-\alpha)]$. As can be inferred from Fig. 4 the corresponding analytical results compare reasonably well with MC data.

A convenient way for visualizing the various dynamic regimes resulting from domain wall and local density fluctuations is the power spectrum

$$I(\omega) \equiv \frac{1}{T}\langle|\Phi(0,\omega)|^2\rangle, \qquad (26)$$

where T is the total time of integration. It is obvious from Figs. 5 and 6 that there are three distinct dynamical regimes.

The DW theory, as described above, fully explains the low-frequency power-law regime $I(\omega) \sim \omega^{-3/2}$. As can easily be shown from specializing Eq. (24) to $x=0$, one finds $I(\omega) \sim L^{-1}\omega^{-3/2}$ [20]. The time window where DW theory is valid ranges from the hopping time $\tau_1 = 1/\mathcal{D}$ to the time needed to travel a distance comparable to the system size
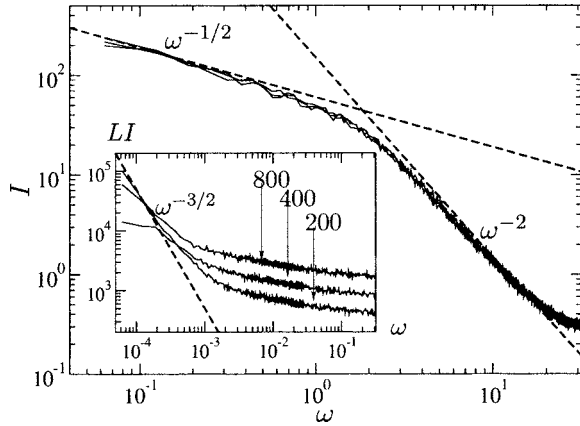
FIG. 6. Power spectrum for systems of 800, 400, and 200 sites and rates $\alpha=\beta=0.4$. Averages are taken over 256 samples. The large-frequency behavior is dominated by local density fluctuations and well described within a BL theory, while the small-frequency regime is dominated by domain wall fluctuations, as a collective mode. Inset: rescaled power spectrum showing the long-time regime dominated by the DW dynamics. When the time scales of the DW and BL dynamics are comparable the separation between the two dynamics, although still present, is not as sharp as in Fig. 5.

$\tau_L \sim L^2/\mathcal{D}$ (note that L is dimensionless). For larger times one expects finite-size effects. In frequency space this corresponds to the domain $[\mathcal{D}/L^2, \mathcal{D}]$.

For frequencies larger than $\omega_1 \gtrsim \mathcal{D}$ the dynamics is dominated by local density fluctuations. Those are well described within BL theory. Note that contrary to the fluctuations of the domain wall, these local density fluctuations are independent of the system size; see Figs. 5 and 6. For time scales larger than the microscopic hopping time of an individual particle (which we have set to 1), one can use the continuum version of the BL theory. Hence for $\omega \lesssim 1$ one expects $I(\omega) \sim \omega^{-1/2}$ which agrees very well with our MC data; note that when $\alpha=\beta \approx 0$ the distinction is clear (Fig. 5), while for $\alpha=\beta \lesssim 1/2$, not only the time scales, but also the amplitudes become comparable since $A=\alpha(1-\alpha)[1-\alpha(1-\alpha)]$ and $C^{\text{DW}}(0,0) \sim (1-2\alpha)^2/4$ [from Eq. (24)]. Therefore (see Fig. 6) the distinction between the BL and DW regimes becomes clearly visible only at very large time (and large systems). At the critical point the amplitude of the DW correlation is identical to zero [see Eq. (23)] and therefore the fluctuations are described by BL in its nonlinear version.

For larger frequencies one has to account for lattice effects. If one applies the lattice version of the BL theory, one finds (see Appendix B)

$$C_k(\omega) = \frac{2[1-\cos(k\pi/L)]A}{\omega^2 + [1-\cos(k\pi/L)]^2}. \tag{27}$$

In order to obtain the power spectrum $C_k(\omega)$ has to be summed over all modes numbers k. The dominant contribution for large frequencies are due to wave vectors close to the zone boundary, $k=L/2$ resulting in a power spectrum $I(\omega) \sim \omega^{-2}$, which is again well confirmed by our MC data (Figs. 5 and 6).

V. CONCLUSIONS

In conclusion we have analyzed the dynamics of the TASEP model over the whole parameter range of exit and entrance rates with emphasis on the behavior in the low- and high-density regimes and the corresponding phase boundary. It turns out that most of the dynamics can be nicely explained in terms of the combined effect of local density fluctuations and collective domain wall motion. The dynamics of the domain wall is determined by the stochasticity in the entrance and exit of particles at the system boundaries. Depending on the parameters this yields to a random walk with or without drift towards the boundaries. For the description of the local density fluctuations we have adopted methods from kinetic theories for electronic transport, known as Boltzmann-Langevin approach. Both the Boltzmann-Langevin and the domain wall approaches are to a large extent phenomenological and hence limited in the range of applicability. Hence we have complemented our studies by extensive Monte Carlo simulations of the TASEP model using the BKL algorithm which allows us to study the real-time dynamics with good accuracy. Our main findings are as follows. For very low densities, the linearized Boltzmann-Langevin theory accounts quantitatively for the shape of the density-density correlations. It becomes less accurate for densities approaching the maximal density of 1/2 as expected from the approximate nature of the theory. Analogous arguments apply for very high densities by virtue of particle-hole symmetry. For densities close to 1/2 linearized Boltzmann-Langevin theory is quantitatively wrong but still captures the main features qualitatively. Exactly at the critical point $\alpha=\beta=1/2$, the full Boltzmann-Langevin theory is identical to the noisy Burgers equation which is known to be in the same universality class as the TASEP model right at this point.

As summarized by the power spectra in Figs. 5 and 6 there is a time-scale separation between the domain wall motion and the local density fluctuations. For frequencies larger than the hopping time of the domain wall $\mathcal{D}$ it is the local density fluctuations which dominate the spectrum. Upon using the continuous and the discrete version of the linearized Boltzmann-Langevin approach we can fully account for the crossover from $\omega^{-1/2}$ to ω^{-2} in the spectrum. For low frequencies $\omega < \mathcal{D}$ domain wall theory gives a power spectrum of $\omega^{-3/2}$ in agreement with the Monte Carlo data.

In summary, two rather elementary approaches, domain wall and Boltzmann-Langevin theories, seem to capture most of the observed dynamics of the TASEP model. This suggests that it may be worthwhile to look for more complex systems which also could be described by these simple methods.
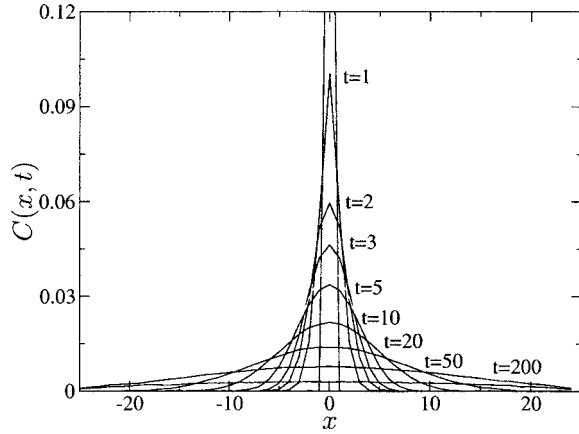
FIG. 7. Time series of the correlation function $C(x,t)$ versus x at the critical point ($\alpha=0.5$ and $\beta=0.5$); the times are indicated in the graph; the system size is $N=50$. Averages are taken over 10^7 samples.

APPENDIX A: CRITICAL POINT $\alpha=\beta=1/2$

For completeness we shortly discuss our results for the correlation function right at the critical point ($\alpha=\beta=1/2$). As can be inferred from Fig. 7 the temporal evolution of its shape is qualitatively and quantitatively different from the low- and high-density phases.

The critical exponents are obtained from a finite-size scaling analysis of the height and width of the correlation function. The insets of Figs. 8(a) and 8(b) show Monte Carlo data for system sizes $N=10$, $N=25$, and $N=50$. These data can be replotted upon using the finite-size scaling relations for the height and width, respectively,

$$C(x=0,t) = L^{2\chi-2}g(t/L^z) = L^{-1}g(t/L^{3/2}), \qquad \text{(A1)}$$

$$W(t) = L^{(2\chi+1)/2}f(t/L^z) = Lf(t/L^{3/2}), \qquad \text{(A2)}$$

which will give us numerical values for the critical exponents.

The critical exponents were determined using an algorithm provided by the authors of Ref. [36]. This code computes and minimizes a sum which weights the distance from an interpolating function based on all the given sequences of data. Errors are extracted measuring the width of the minimum of such function (which has been tested to be zero if the values are exact). From this we obtain for the autocorrelation (peak) $2\chi=0.98\pm0.03$ and $z=1.52\pm0.02$ and, consistently, $2\chi=0.92\pm0.09$ and $z=1.53\pm0.08$ for the width. It constitutes direct numerical evidence for the system belonging to the KPZ universality class ($2\chi=1$ and $z=3/2$), as expected from earlier analytical results for periodic systems. Our measurements confirm the numerical results in Ref. [37].
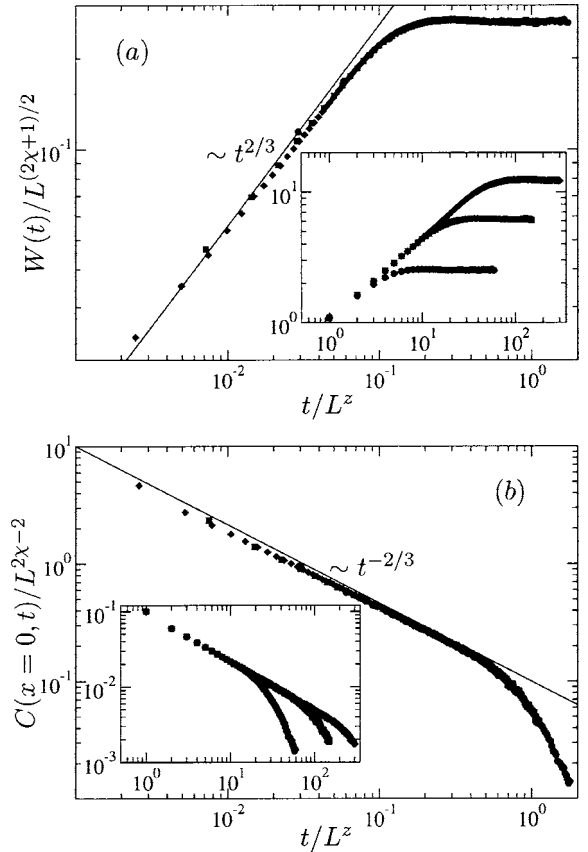

FIG. 8. (a) Width of the correlation function and (b) autocorrelation. Averages are computed using 10^7 samples at the critical point $\alpha=\beta=1/2$. The data are rescaled according to Eqs. (A2) and (A1) with the exponents presented in the text. Insets show the plots before rescaling.

APPENDIX B: ANALYSIS OF THE BOLTZMANN-LANGEVIN EQUATION ON A DISCRETE LATTICE

In this appendix we study the time behavior of the correlation function at short times in the regime where the discreteness of the system plays a major role. We use $\phi_n(t)=\delta\rho_n(t)$ as the discrete equivalent of the field $\phi(x,t)$. We can write an equation of motion for the correlation function multiplying Eq. (5) by ϕ_n^0:

$$\frac{d\langle\phi_n\phi_n^0\rangle}{dt} = \langle\phi_{n-1}\phi_n^0\rangle(1-\alpha) - \langle\phi_n\phi_n^0\rangle + \alpha\langle\phi_{n+1}\phi_n^0\rangle - \langle\eta_n\phi_n^0\rangle$$

$$+ \langle\eta_{n-1}\phi_n^0\rangle, \qquad \text{(B1)}$$

where $\bar{\rho}=\alpha$ and we neglect the nonlinear terms. This system of equations involves two-point correlation functions for three different lattice sites, but can be written in a closed form (at least for short time regimes) by assuming that (i) $\langle\eta_n\phi_n^0\rangle=0$, which makes sense, the noise being independent of the dynamics itself; (ii) $\langle\phi_{n-2}\phi_n^0\rangle=0$, which is reasonable for a short time; and (iii) $\langle\phi_m^0\phi_n^0\rangle=\frac{1}{4}\delta_{mn}$ [this originates the sharp tip in $C(x,t)$].

The central site of the system will be considered the reference site ($n=0$). Defining $C_i(t) \equiv \langle \phi_{n+i}(t)\phi_n^0 \rangle$ we rewrite Eq. (B1) as

$$\frac{dC_0}{dt} = (1-\alpha)C_{-1} - C_0 + \alpha C_{+1}. \qquad (B2)$$

By analogous reasoning, multiplying Eq. (B1) for ϕ_{n-1} and ϕ_{n+1}, we find a system of linear differential equations:

$$\frac{d\vec{v}(t)}{dt} = \hat{M}\vec{v}(t), \qquad (B3)$$

with $\vec{v}=(C_{-1},C_0,C_{+1})^t$ and

$$\hat{M} = \begin{bmatrix} -1 & \alpha & 0 \\ 1-\alpha & -1 & \alpha \\ 0 & 1-\alpha & -1 \end{bmatrix}.$$

For the initial condition $\vec{v}_0=(0,1/4,0)^t$ the solution $\vec{v}(t)=\exp(\hat{M}t)\vec{v}_0$ leads to

$$C_0(t) = \frac{1}{4}e^{-t}\cosh[t\sqrt{2\alpha(1-\alpha)}] = \frac{1}{4} - \frac{1}{4}t + \frac{1}{4}\left(\frac{1}{2}+\alpha-\alpha^2\right)t^2$$

$$+ O(t^3). \qquad (B4)$$

At short time the autocorrelation decays linearly in time from a constant value ($1/4$), while the other terms grow linearly:

$$C_{-1}(t) = \frac{1}{4}\sqrt{\frac{\alpha}{1(1-\alpha)}}e^{-t}\sinh[t\sqrt{2\alpha(1-\alpha)}]$$

$$= \frac{\alpha}{4}t - \frac{\alpha}{4}t^2 + O(t^3), \qquad (B5)$$

$$C_{+1}(t) = C_{+1} = \frac{1}{4}\sqrt{\frac{1-\alpha}{2\alpha}}e^{-t}\sinh[t\sqrt{2\alpha(1-\alpha)}]$$

$$= \frac{(1-\alpha)}{4}t - \frac{1-\alpha}{4}t^2 + O(t^3). \qquad (B6)$$

Note that even relaxing hypothesis (ii), assuming therefore $C_{\pm 2} \neq 0$, and dealing with a larger matrix $\hat{M}$, one does not find correction to the leading behavior in time for $C_0(t)$, since correlation functions for more distant sites, such as $C_{\pm 2}$, scale as $C_{\pm 2} \sim t^2$.

In order to look at the behavior in frequency space, we apply the BL scheme in the discrete lattice and extrapolate the regime of the correlation function at large ω. Let us start from the real space-time Boltzmann-Langevin equation (5) and let us introduce the discrete Fourier transform $\phi_k = \sum_{n=-L/2}^{L/2} \phi_n e^{ikn\pi/L}$ where k indicates the mode number. In order to express the linearized BL equation in discrete Fourier space, we multiply Eq. (5) by $e^{ikn\pi/L}$ and sum over n. Even though the system is not translational invariant, in this limit the system can be considered as infinite and we do not take care of the boundaries. Performing a Fourier transform in time we get the discrete equivalent of Eq. (8):

$$\left[i\left(\omega + 2\alpha\sin\frac{k\pi}{L}\right) + (1-e^{ik\pi/L})\right]\phi_k(\omega) = \eta_k(\omega)(1-e^{ik\pi/L})$$

$$(B7)$$

and find the correlation function

$$C_k(\omega) = \frac{2A[1-\cos(k\pi/L)]}{[\omega - v\sin(k\pi/L)]^2 + [1-\cos(k\pi/L)]^2}, \quad (B8)$$

where we use the notation $v=1-2\alpha$ and $A=\alpha[1-\alpha(1-\alpha)]$ as done above.

The autocorrelation is the sum over all the modes, but the dominant contribution for large frequencies is due to wave vectors close to the zone boundary, $k=L/2$:

$$C(x=0,\omega) \simeq \frac{1}{L}\sum_{k=0}^{L-1} \frac{2A[1-\cos(k\pi/L)]}{\omega^2} = 2A\omega^{-2}, \quad (B9)$$

which (by the Wiener-Khinchin theorem) is the power spectrum mentioned in Sec. IV B.

[1] C. MacDonald, J. Gibbs, and A. Pipkin, Biopolymers **6**, 1 (1968).

[2] A. Parmeggiani, T. Franosch, and E. Frey, Phys. Rev. Lett. **90**, 086601 (2003).

[3] R. Lipowsky, S. Klumpp, and T. Nieuwenhuizen, Phys. Rev. Lett. **87**, 108101 (2001).

[4] D. Chowdhury, L. Santen, and A. Schadschneider, Phys. Rep. **329**, 199 (2000).

[5] Q. Wei, C. Bechinger, and P. Leiderer, Science **287**, 625 (2000).

[6] R. Willmann, G. Schütz, and D. Challet, J. Phys. A **316**, 413 (2002).

[7] B. Derrida, Phys. Rep. **301**, 65 (1998).

[8] G. Schütz, *Exactly solvable models in many-body systems, Vol. 19 of Phase Transition and Critical Phenomena* (Academic Press, London, 2001).

[9] B. Derrida, E. Domany, and D. Mukamel, J. Stat. Phys. **69**, 667 (1992).

[10] G. Schütz and E. Domany, J. Stat. Phys. **72**, 277 (1993).

[11] B. Derrida, M. Evans, V. Hakim, and V. Pasquier, J. Phys. A **26**, 1493 (1993).

[12] D. Dhar, Phase Transitions **9**, 1 (1987).

[13] L. H. Gwa and H. Spohn, Phys. Rev. A **46**, 844 (1992).

[14] B. Derrida, M. Evans, and D. Mukamel, J. Phys. A **26**, 4911 (1993).

[15] B. Derrida, J. Lebowitz, and E. Speer, Phys. Rev. Lett. **87**,

150601 (2001).

[16] U. Bilstein and B. Wehefritz, J. Phys. A **30**, 4925 (1997).

[17] M. Dudziński and G. Schütz, J. Phys. A **33**, 8351 (2000).

[18] Z. Nagy, C. Appert, and L. Santen, J. Stat. Phys. **109**, 623 (2002).

[19] A. Kolomeisky, G. Schütz, E. Kolomeisky, and J. Straley, J. Phys. A **31**, 6911 (1998).

[20] S. Takesue, T. Mitsudo, and H. Hayakawa, Phys. Rev. E **68**, 015103(R) (2003).

[21] J. L. Lebowitz, E. Presutti, and H. Spohn, J. Stat. Phys. **51**, 841 (1988).

[22] H. van Beijeren, R. Kutner, and H. Spohn, Phys. Rev. Lett. **54**, 2026 (1985).

[23] D. Forster, D. R. Nelson, and M. J. Stephen, J. Phys. A **16**, 732 (1977).

[24] M. Kogan and A. Y. Shul'man, Sov. Phys. JETP **29**, 3 (1969).

[25] S. Kogan, *Electronic Noise and Fluctuations in Solids* (Cambridge University Press, New York, 1996).

[26] Y. Blanter and M. Büttiker, Phys. Rep. **336**, 1 (2000).

[27] M. Doi, J. Phys. A **9**, 1465 (1976).

[28] P. Grassberger and M. Scheunert, Fortschr. Phys. **28**, 547 (1980).

[29] L. Peliti, J. Phys. (Paris) **46**, 1469 (1985).

[30] J. Krug, Phys. Rev. Lett. **67**, 1882 (1991).

[31] M. Kardar, G. Parisi, and Y. C. Zhang, Phys. Rev. Lett. **56**, 889 (1986).

[32] N. Goldenfeld, *Lecture on Phase Transition and the Renormalization Group*, Frontiers of Physics (Westview Press, Co, 1992).

[33] A. Bortz, M. Kalos, and J. Lebowitz, J. Comput. Phys. **17**, 10 (1975).

[34] D. Landau and K. Binder, *Monte Carlo Simulations in Statistical Physics* (Cambridge University Press, Cambridge, England, 2000).

[35] M. Schwarz and D. Poland, J. Chem. Phys. **63**, 557 (1975).

[36] S. Bhattacharjee and F. Seno, J. Phys. A **34**, 6375 (2001).

[37] R. Juhász and L. Santen, J. Phys. A **37**, 3933 (2004).